Editors' Suggestion | Featured in Physics

Electronic Spectrum of Twisted Graphene Layers under Heterostrain

Loïc Huder,[1] Alexandre Artaud,[1,2] Toai Le Quang,[1] Guy Trambly de Laissardière,[3] Aloysius G. M. Jansen,[1] Gérard Lapertot,[1] Claude Chapelier,[1] and Vincent T. Renard[1]

[1]*Université Grenoble Alpes, CEA, INAC, PHELIQS, F-38000 Grenoble, France*

[2]*Université Grenoble Alpes, CNRS, Institut NEEL, F-38000 Grenoble, France*

[3]*Laboratoire de Physique Théorique et Modélisation, Université de Cergy-Pontoise-CNRS, F-95302 Cergy-Pontoise, France*

(Received 8 December 2017; revised manuscript received 12 February 2018; published 12 April 2018)

We demonstrate that stacking layered materials allows a strain engineering where each layer is strained independently, which we call heterostrain. We combine detailed structural and spectroscopic measurements with tight-binding calculations to show that small uniaxial heterostrain suppresses Dirac cones and leads to the emergence of flat bands in twisted graphene layers (TGLs). Moreover, we demonstrate that heterostrain reconstructs, much more severely, the energy spectrum of TGLs than homostrain for which both layers are strained identically, a result which should apply to virtually all van der Waals structures opening exciting possibilities for straintronics with 2D materials.

DOI: 10.1103/PhysRevLett.120.156405

A variety of new electronic, optoelectronic, and photovoltaic devices are produced by stacking different two-dimensional materials into van der Waals heterostructures [1,2]. Radical effects on the electronic properties can also be achieved by stacking identical materials into van der Waals homostructures. This is well illustrated by graphene bilayers [3] and transition metal dichalcogenide bilayers [4] which are drastically different from their monolayer counterpart. The properties of van der Waals structures and devices not only depend on the choice of materials, but also on the details of the stacking which offers additional degrees of freedom [2]. The rotation angle between the layers has been exploited to tune the van Hove singularities in twisted graphene layers (TGLs) [5–13], to achieve the first experimental observation of the Hofstadter butterfly in graphene on h-BN [14,15], and to uncover correlated insulating and superconducting states in magic angle twisted graphene layers [16,17]. It has also allowed monitoring the optical responses of transition metal dichalcogenide homo-[18] and heterostructures [19]. Strain, originating from external stress [20–23] or from interlayer interactions [24–26] is another degree of freedom.

In this letter, we have studied the effect of homogeneous heterostrain on electronic properties of TGLs. Here, the layers experience different and independent homogeneous in-plane strain, a situation which has no equivalent in bulk materials where covalent bonds link atoms on both sides of the junction. Heterostrain is possible in 2D stacks because independent deformations on each side of the interface are allowed by the weak interlayer van der Waals bonding. The effect of strain on the structure of TGLs is sketched in Fig. 1. In the absence of strain [Fig. 1(a)], the TGLs show a typical moiré pattern resulting from the superposition of the two atomic lattices. With uniaxial strain applied identically to both layers (homostrain), the moiré is slightly deformed [Fig. 1(b)]. The moiré appears to be much more affected by a similar deformation of the top layer only [heterostrain is illustrated in Fig. 1(c)]. This magnifying effect of the moiré has been recently shown to allow for the determination of heterostrain [27–30], and a strong influence on the moiré physics was predicted [27]. Since TGLs, like other van der Waals structures, inherit their band structure from the moiré potential, one may wonder whether this apparently large influence of heterostrain on the moiré also has strong implications for their electronic properties.

Figures 1(d) and 1(e) demonstrate that this is, indeed, the case. Figure 1(d) shows a constant-current scanning tunnelling microscope (STM) image of a TGL structure on SiC $(000\bar{1})$ obtained using the growth recipe described in Ref. [31]. The image shows a moiré pattern similar to those depicted in Figs. 1(a), 1(b), and 1(c). The contrast results from alternation of *AA*-stacked regions, where the layers are in perfect registry (bright regions in the STM image) and of *AB*-stacked regions where the layer stacking is similar to graphite (dark regions in the image). Figure 1(e) shows the differential conductance dI/dV which is proportional to the local density of states LDOS. The differential conductance in *AA* and *AB* regions was recorded as a function of the applied bias voltage V using phase sensitive detection (2 mV modulation of the bias voltage at 263 Hz. See Supplemental Material [32] Section A for more details about reproducibility and spatial dependence of the data). The measurements were performed at $T = 50$ mK. The most striking feature is the presence of a group of resonances (E_1', E_0, E_1) located near zero energy which are much more intense in *AA* regions. The linear extrapolation of the LDOS at high energy (dashed line) allows us to deduce that this group of states is centered around $E = -25$ meV which

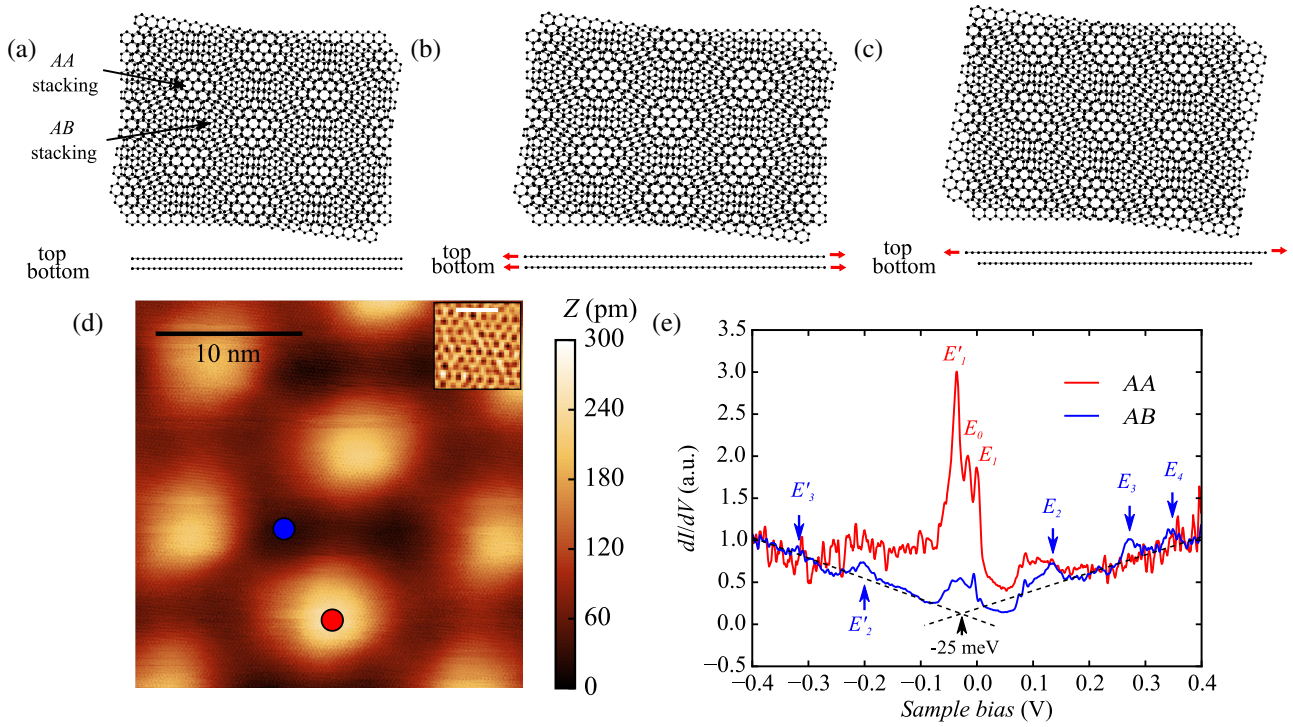

FIG. 1. Strained twisted graphene layers. (a), (b), and (c) Sketch of TGLs without or with strain; top and side views. Red arrows in the side views indicate the presence of strain in each layer. (a) TGLs without strain. (b) TGLs with 10% of uniaxial strain applied to both layers. (c) TGLs with 10% of uniaxial strain applied to the top layer only. (d) 26.4×26.4 nm^2 topograph of twisted graphene layers showing the moiré pattern. The twist angle between the graphene layers was estimated to be $\theta = 1.25°$. Bias voltage $V = -400$ mV and current set point $I = 50$ pA. Inset: Zoom of the image showing the honeycomb lattice of the carbon atoms in the top layer. The scale bar is 1 nm. (e) Differential conductance (dI/dV) recorded at the spots marked with colored dots in Fig. 1(a) (red and blue dots for *AA* and *AB* regions, respectively) showing multiple resonances in *AA* regions (red arrows) and well resolved peaks at higher energy in *AB* regions (blue arrows). Bias voltage $V = -400$ mV and current set point $I = 300$ pA. The doping is estimated from the linear extrapolation of the high-energy density of states (dashed lines).

corresponds to the typical doping of graphene grown on the carbon-face of SiC [43]. These three resonances are surprising since TGLs usually present only two resonances (van Hove singularities) flanking the Dirac point [5–13], and we will show that this qualitative difference can be attributed to the modification of the band structure by a small heterostrain.

A detailed Fourier analysis [28] of the image in Fig. 1(d) reveals that the layers are rotated by 1.25° and, more importantly, that one layer is slightly strained with respect to the other layer. This heterostrain consists of a combination of a small uniaxial heterostrain $\varepsilon_{\mathrm{uni}}^{\mathrm{het}} = 0.35\%(\pm 0.03\%)$ applied along the horizontal direction in Fig. 1(d) and an even smaller biaxial heterostrain $\varepsilon_{\mathrm{bi}}^{\mathrm{het}} = -0.06\%(\pm 0.005\%)$ (see Supplemental Material [32] Sec. B for the detailed analysis, including Refs. [33,34]). We note that possible local deformations are ignored by the Fourier analysis since it is performed on the entire image of Fig. 1(d). The above values correspond to a spatially averaged heterostrain. This small heterostrain originates from the pinning of the top layer at its boundaries during the growth. It is substantiated by moiré lattice deformations at the boundary of the grain studied (see Supplemental Material [32] Sec. C for more details).

We have theoretically investigated the influence of this small heterostrain on the electronic properties. Local densities of states are computed by recursion method in real space from a tight-binding Hamiltonian with Slater-Koster parameters for p_z orbitals (see Supplemental Material [32] Sec. D, including Refs. [35–38]). Hopping parameters depend on distance between orbitals, and thus, the same parameters are used in bilayer with and without strain, whatever the rotation angle. These parameters have been determined previously to simulate the dependence of van Hove singularities on the twist angle [12]. In addition to providing structural information, the Fourier analysis outputs a commensurate approximate of the experimental structure which can be used for tight-binding calculations (see Supplemental Material [32] Sec. E). The top panel of Fig 2(a) displays the corresponding calculated LDOS. This calculation reproduces the three resonances seen in the measurements of Fig. 1(e). For comparison, Fig. 2(b) shows the calculated LDOS of a similar commensurate approximate with the same rotation angle but exempt of heterostrain. In this case, the only two resonances are van Hove singularities arising from saddle points in the lowest

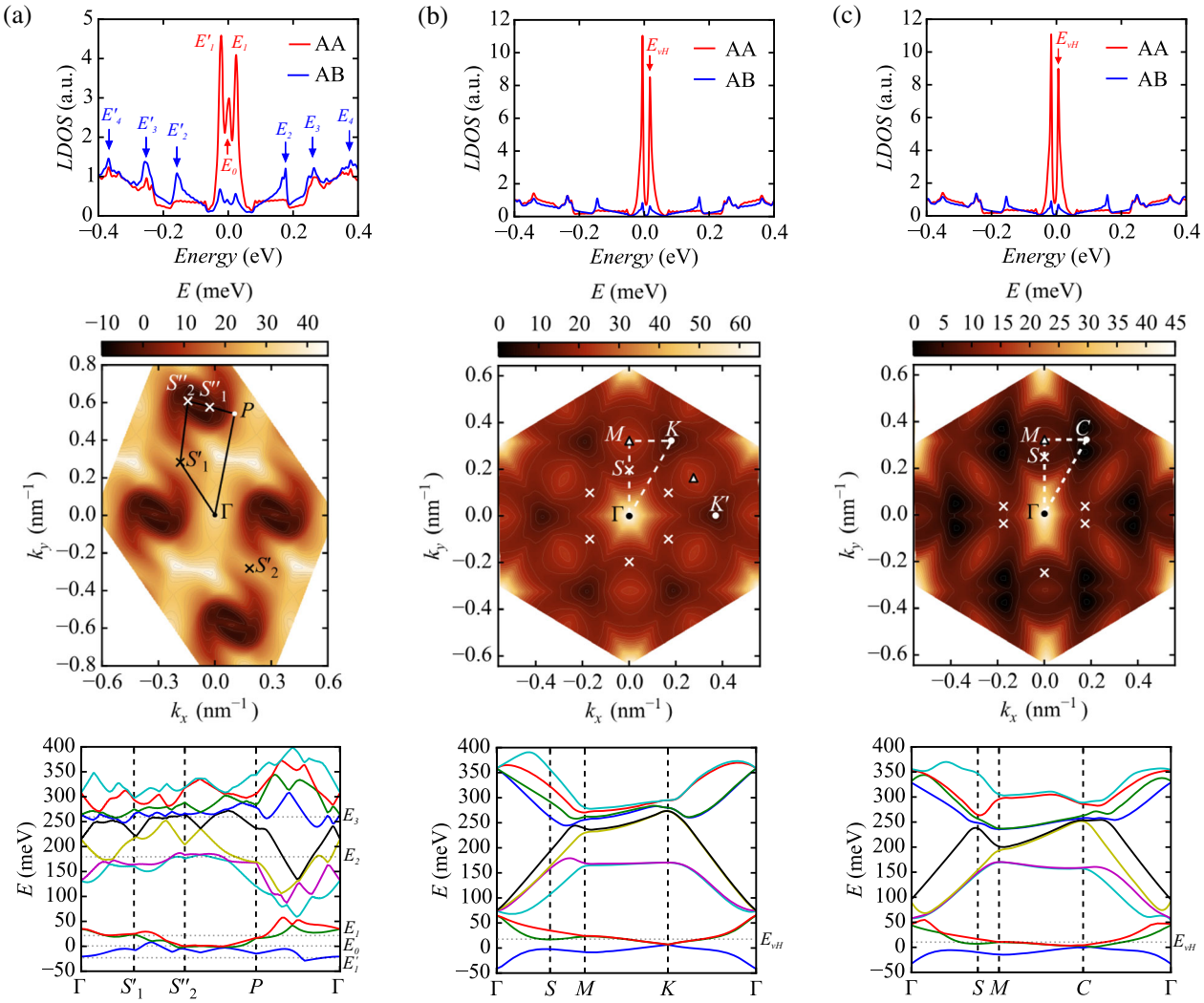

FIG. 2. Tight binding calculations with and without strain. The figure is organized in columns. In each column, the upper panel shows the LDOS in *AA* and *AB* regions. The middle panel shows the calculated energy map of the first band above E_F (Crosses indicate saddle points). Lines correspond to the trajectory of the cuts in the band structure presented in the lower panel which shows the dispersion of the valence band and the first ten bands above E_F. (a) Result for the structure with heterostrain of 0.35% corresponding to the experimental situation. (b) Result for the unstrained structure with a twist angle close to the experimental situation. (c) Result for the same structure as panel (b) with a homostrain of 0.35%. In the lower part of panel (c), for simplicity, we have plotted cuts in ΓC and MC since the degeneracy at K and K' points is lifted by homostrain as pointed out in Ref. [21] .

energy bands [5–13]. The saddle points, marked by crosses in the central panel of Fig. 2(b), generate the positive energy singularity. The negative energy singularity is related to similar saddle points in the first negative energy band. The central panel of Fig. 2(a) shows that this band is completely reconstructed by heterostrain. The threefold symmetry is lost and there are no longer Dirac points. Weakly dispersing regions appear around points S_1'' and S_2'' from which the zero energy resonance E_0 originates. The resonance at E_1 comes from the saddle points S_1' and S_2' and the resonance E_1' comes from similar features in the first negative energy band. Cuts in the band structure presented in the lower panels of Figs. 2(a) and 2(b) demonstrate that the entire band structure is modified by the small heterostrain. Despite being undetectable by visual inspection of Fig. 1(d), heterostrain has, nevertheless, profound consequences.

Interestingly, heterostrain does not suppress the electronic localization induced by the moiré potential [8–10]. Indeed, the central peaks in the LDOS are much more pronounced in *AA* regions than in *AB* regions in both experiments and calculations. Contrary to E_1', E_0, E_1, the high energy resonances (E_2, E_3, E_4) in Fig. 1(e), which are associated with a partial band gap opening in higher energy moiré bands [9,13], are localized in *AB* regions. This finding, which has never been reported, is well reproduced by tight binding. Further theoretical work is needed to understand its origin.

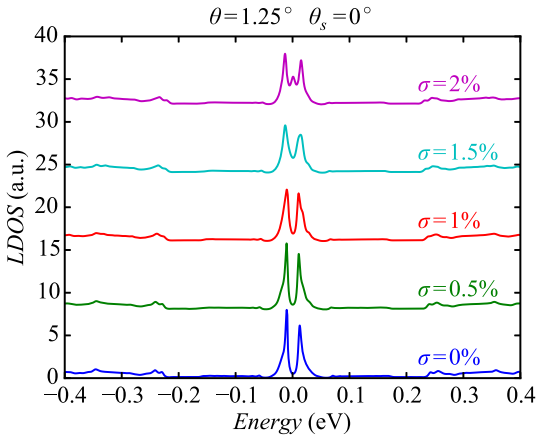

FIG. 3. Calculated LDOS with homostrain. Calculated LDOS in *AA* regions for the commensurate structure with $\theta = 1.25°$ for different uniaxial homostrain magnitudes along the zigzag direction of the bottom layer. All curves have been shifted vertically for clarity.

As a final verification, we have investigated the effect of homostrain since previous tight-binding calculations [21] have shown that homostrain can also alter the band structure of TGLs with large rotation angles. For consistent comparison between homo- and heterostrain, we performed tight-binding calculations with 0.35% of uniaxial homostrain applied in the x direction to the layers rotated by 1.25° (details of the calculations are in the Supplemental Material [32] Sec. F, including Ref. [39]). Figure 2(c) shows that, in this case, the LDOS is similar to the unstrained situation and the band structure is only weakly affected. This has to be expected since, as the layers are stretched together, the interlayer relative atomic positions evolve much slower than for heterostrain. This is why much larger values of homostrain (2%) would be required to reproduce our experimental LDOS (see Fig. 3). Such strain is much larger than observed by Raman in our sample (see Supplemental Material [32] Sec. G, including Refs. [40–42]) and is usually reported for graphene on SiC [44]. As a consequence, we exclude homostrain as the origin of our observations.

In conclusion, the properties of TGLs depend on the electronic coupling of the layers and, hence, on their relative arrangement. Heterostrain is, therefore, particularly efficient for tuning their band structure. This should be the case of other homostructures (MoS_2, WS_2, WSe_2, etc.) and heterostructures (Gr/h-BN, $MoSe_2/WSe_2$, etc.) in which interlayer electronics also has a strong influence. In the future, a whole new generation of electronic devices could arise exploiting heterostrain in van der Waals stacks with intentionally individually strained layers. It could prove instrumental in the exploration of the recently discovered strongly correlated electron physics in carbon materials [16,17,45].

T. L. Q. was supported by a CIBLE Fellowship from Region Rhone-Alpes. We thank Valérie Reita and optics and microscopy technological group for valuable support on Raman spectroscopy. The authors wish to thank Johann Coraux for fruitful discussions.

[1] A. K. Geim and I. V. Grigorieva, Nature (London) **499**, 419 (2013).
[2] K. S. Novoselov, A. Mishchenko, A. Carvalho, and A. H. C. Neto, Science **353**, aac9439 (2016).
[3] T. Ohta, A. Bostwick, T. Seyller, K. Horn, and E. Rotenberg, Science **313**, 951 (2006).
[4] K. F. Mak, C. Lee, J. Hone, J. Shan, and T. F. Heinz, Phys. Rev. Lett. **105**, 136805 (2010).
[5] L. Van Hove, Phys. Rev. **89**, 1189 (1953).
[6] J. M. B. Lopes dos Santos, N. M. R. Peres, and A. H. Castro Neto, Phys. Rev. Lett. **99**, 256802 (2007).
[7] G. Li, A. Luican, J. M. B. Lopes dos Santos, A. H. Castro Neto, A. Reina, J. Kong, and E. Y. Andrei, Nat. Phys. **6**, 109 (2010).
[8] G. T. de Laissardière, D. Mayou, and L. Magaud, Nano Lett. **10**, 804 (2010).
[9] R. Bistritzer and A. H. MacDonald, Proc. Natl. Acad. Sci. U.S.A. **108**, 12233 (2011).
[10] J. M. B. Lopes dos Santos, N. M. R. Peres, and A. H. Castro Neto, Phys. Rev. B **86**, 155449 (2012).
[11] G. T. de Laissardière, D. Mayou, and L. Magaud, Phys. Rev. B **86**, 125413 (2012).
[12] I. Brihuega, P. Mallet, H. González-Herrero, G. T. de Laissardière, M. M. Ugeda, L. Magaud, J. M. Gómez-Rodríguez, F. Ynduráin, and J.-Y. Veuillen, Phys. Rev. Lett. **109**, 196802 (2012).
[13] D. Wong, Y. Wang, J. Jung, S. Pezzini, A. M. DaSilva, H.-Z. Tsai, H. S. Jung, R. Khajeh, Y. Kim, J. Lee, S. Kahn, S. Tollabimazraehno, H. Rasool, K. Watanabe, T. Taniguchi, A. Zettl, S. Adam, A. H. MacDonald, and M. F. Crommie, Phys. Rev. B **92**, 155409 (2015).
[14] C. R. Dean, L. Wang, P. Maher, C. Forsythe, F. Ghahari, Y. Gao, J. Katoch, M. Ishigami, P. Moon, M. Koshino, T. Taniguchi, K. Watanabe, K. L. Shepard, J. Hone, and P. Kim, Nature (London) **497**, 598 (2013).
[15] L. A. Ponomarenko, R. V. Gorbachev, G. L. Yu, D. C. Elias, R. Jalil, A. A. Patel, A. Mishchenko, A. S. Mayorov, C. R. Woods, J. R. Wallbank, M. Mucha-Kruczynski, B. A. Piot, M. Potemski, I. V. Grigorieva, K. S. Novoselov, F. Guinea, V. I. Fal'ko, and A. K. Geim, Nature (London) **497**, 594 (2013).
[16] Y. Cao, V. Fatemi, S. Fang, K. Watanabe, K. Taniguchi, E. Kaxiras, and P. Jarillo-Herrero, arXiv:1803.02342 [Nature (London) (to be published)].
[17] Y. Cao, V. Fatemi, A. Demir, S. Fang, S. L. Tomarken, J. Y. Luo, J. D. Sanchez-Yamagishi, K. Watanabe, K. Taniguchi, E. Kaxiras, R. C. Ashoori, and P. Jarillo-Herrero, arXiv:1802.00553 [Nature (London) (to be published)].
[18] K. Liu, L. Zhang, T. Cao, C. Jin, D. Qiu, Q. Zhou, A. Zettl, P. Yang, S. G. Louie, and F. Wang, Nat. Commun. **5**, 4966 (2014).
[19] P. K. Nayak, Y. Horbatenko, S. Ahn, G. Kim, J.-u. Lee, A.-r. Jang, H. Lim, D. Kim, S. Ryu, H. Cheong, N. Park, and H. S. Shin, ACS Nano **11**, 4041 (2017).

[20] W. Yan, W.-Y. He, Z.-D. Chu, M. Liu, L. Meng, R.-F. Dou, Y. Zhang, Z. Liu, J.-C. Nie, and L. He, Nat. Commun. **4**, 2159 (2013).
[21] V. H. Nguyen and P. Dollfus, 2D Mater. **2**, 035005 (2015).
[22] Y. He, Y. Yang, Z. Zhang, Y. Gong, W. Zhou, Z. Hu, G. Ye, X. Zhang, E. Bianco, S. Lei, Z. Jin, X. Zou, Y. Yang, Y. Zhang, E. Xie, J. Lou, B. Yakobson, R. Vajtai, B. Li, and P. Ajayan, Nano Lett. **16**, 3314 (2016).
[23] F. Huang, B. Cho, H.-s. Chung, S. B. Son, J. H. Kim, T.-s. Bae, H. J. Yun, J. I. Sohn, K. H. Oh, M. G. Hahm, J. H. Park, and W.-k. Hong, Nanoscale **8**, 17598 (2016).
[24] C. R. Woods *et al.*, Nat. Phys. **10**, 451 (2014).
[25] J. Jung, A. M. Dasilva, A. H. Macdonald, and S. Adam, Nat. Commun. **6**, 6308 (2015).
[26] H. Kumar, D. Er, L. Dong, J. Li, and V. B. Shenoy, Sci. Rep. **5**, 10872 (2015).
[27] D. A. Cosma, J. R. Wallbank, V. Cheianov, and V. I. Fal'ko, Faraday Discuss. **173**, 137 (2014).
[28] A. Artaud, L. Magaud, T. Le Quang, V. Guisset, P. David, C. Chapelier, and J. Coraux, Sci. Rep. **6**, 25670 (2016).
[29] A. Summerfield, A. Davies, T. S. Cheng, V. V. Korolkov, Y. Cho, C. J. Mellor, C. T. Foxon, A. N. Khlobystov, K. Watanabe, T. Taniguchi, L. Eaves, S. V. Novikov, and P. H. Beton, Sci. Rep. **6**, 22440 (2016).
[30] Y. Jiang, J. Mao, J. Duan, X. Lai, K. Watanabe, T. Taniguchi, and E. Y. Andrei, Nano Lett. **17**, 2839 (2017).
[31] B. Kumar, M. Baraket, M. Paillet, J.-R. Huntzinger, A. Tiberj, A. Jansen, L. Vila, M. Cubuku, C. Vergnaud, M. Jamet, G. Lapertot, D. Rouchon, A.-A. Zahab, J.-L. Sauvajol, L. Dubois, F. Lefloch, and F. Duclairoir, Physica (Amsterdam) **75E**, 7 (2016).
[32] See Supplemental Material at http://link.aps.org/supplemental/10.1103/PhysRevLett.120.156405 for more information on the reproducibility of the data, the Fourier analysis, the origin of heterostrain, tight binding calculations, the effect of homostrain and Raman measurements, which includes Refs. [33–42].
[33] R. L. Park and H. H. Madden, Surf. Sci. **11**, 188 (1968).
[34] P. Zeller, X. Ma, and S. Günther, New J. Phys. **19**, 013015 (2017).
[35] V. Cherkez, G. T. de Laissardière, P. Mallet, and J.-Y. Veuillen, Phys. Rev. B **91**, 155428 (2015).
[36] J. C. Slater and G. F. Koster, Phys. Rev. **94**, 1498 (1954).
[37] A. H. Castro Neto, F. Guinea, N. M. R. Peres, K. S. Novoselov, and A. K. Geim, Rev. Mod. Phys. **81**, 109 (2009).
[38] R. Haydock, V. Heine, and M. J. Kelly, J. Phys. C **5**, 2845 (1972).
[39] O. L. Blakslee, D. G. Proctor, E. J. Seldin, G. B. Spence, and T. Weng, J. Appl. Phys. **41**, 3373 (1970).
[40] A. C. Ferrari and D. M. Basko, Nat. Nanotechnol. **8**, 235 (2013).
[41] R. W. Havener, H. Zhuang, L. Brown, R. G. Hennig, and J. Park, Nano Lett. **12**, 3162 (2012).
[42] A. Das, S. Pisana, B. Chakraborty, S. Piscanec, S. K. Saha, U. V. Waghmare, K. S. Novoselov, H. R. Krishnamurthy, A. K. Geim, A. C. Ferrari, and A. K. Sood, Nat. Nanotechnol. **3**, 210 (2008).
[43] D. Sun, C. Divin, C. Berger, W. A. de Heer, P. N. First, and T. B. Norris, Phys. Rev. Lett. **104**, 136802 (2010).
[44] T. E. Beechem, T. Ohta, B. Diaconescu, and J. T. Robinson, ACS Nano **8**, 1655 (2014).
[45] K. Kim, A. DaSilva, S. Huang, B. Fallahazad, S. Larentis, T. Taniguchi, K. Watanabe, B. J. LeRoy, A. H. MacDonald, and E. Tutuc, Proc. Natl. Acad. Sci. U.S.A. **114**, 3364 (2017).